Title

Decoding unconscious events and their transition to a unified percept in visual spatio-temporal integration

Maëlan Q. Menétrey[1,2,3], Michael H. Herzog[1], & David Pascucci[1,2,3]

[1]Laboratory of Psychophysics, Brain Mind Institute, École Polytechnique Fédérale de Lausanne (EPFL), Lausanne, Switzerland

[2]Psychophysics and Neural Dynamics Lab, Department of Radiology, Lausanne University Hospital (CHUV) and University of Lausanne (UNIL), Lausanne, Switzerland

[3]The Sense Innovation and Research Center, Lausanne, Switzerland

Keywords: unconscious processing, conscious perception, neural correlates, EEG decoding

Corresponding author: maelan.menetrey@gmail.com

Number of pages: 40

Number of figures: 6; of supplementary figure: 1

Number of words for abstract: 161; for introduction: 505; for results: 1999; for discussion: 1888

Funding: This work was supported by the Swiss National Science Foundation (grant number 325130_204898; grant numbers PZ00P1_179988 and PZ00P1_179988/2; and grant number TMSGI1_218247).

Abstract

In postdictive effects, where later events influence the perception of earlier ones, conscious perception is preceded by extended periods of unconscious processing. This is evident in the Sequential Metacontrast (SQM) paradigm, in which vernier offsets are unconsciously integrated over several hundred milliseconds. Regardless of whether one or multiple verniers are shown, only a single offset is perceived along a motion stream. The SQM, along with other postdictive phenomena, thus provides a unique opportunity to dissociate unconscious from conscious stages of visual processing, as these stages are well separated in time. Using EEG during the SQM, we identified two distinct stages of neural activity: an early occipital EEG activity pattern (~200 ms after the initial vernier) associated with unconscious processing, and a later centro-parietal EEG pattern (~400-600 ms after SQM onset) associated with the integrated percept and behavioral report. We propose that the transition between these neural patterns marks the shift from unconscious encoding of individual visual stimuli to their integrated percept.

Introduction

Conscious perception feels like a continuous stream—we seem to experience the world at each moment of time. However, several visual phenomena challenge this idea. For instance, in a classic apparent motion phenomenon, two dots of different colors are flashed at separate locations with a brief delay (Kolers & Von Grünau, 1976). Rather than perceiving two distinct flashes one after the other, we perceive a single moving dot that changes color midway. Logically, the color change can only be perceived after the second dot is presented, implying that later events influence how we perceive earlier ones. These postdictive effects provide a unique opportunity to study the neural correlates of both conscious and unconscious processing, as well as the transitions between the two, using high-temporal resolution imaging techniques like electroencephalography (EEG).

A prime tool for studying these processes is the Sequential Metacontrast (SQM) paradigm (Figures 1A and 1B). In this paradigm, a sequence of vertical lines is presented, creating the illusion of two diverging motion streams expanding from a central point (Otto et al., 2009, 2010). When one of the lines contains a horizontal vernier offset, all the other lines are perceived as having the same offset, even though they are actually straight. When the stream contains two vernier stimuli with opposite offsets, the offsets integrate mandatorily: observers

are unable to report the individual offsets separately or which specific lines carry offsets (Drissi-Daoudi et al., 2019). Instead, they perceive only a single offset (Menétrey et al., 2023). Thus, multiple offsets are integrated unconsciously, and only the final, integrated offset reaches conscious perception.

In the SQM, the mandatory integration period of the vernier offsets is approximately 330-450 ms, depending on the observer and the condition (Vogelsang et al., 2023, 2024). When two offsets are separated by more than ~ 450 ms, observers can report the offsets individually (Drissi-Daoudi et al., 2019; Vogelsang et al., 2023). These findings suggest that the brain integrates features within a relatively long-lasting window of unconscious processing, followed by an integrated conscious percept (Herzog et al., 2016, 2020). The existence of such long-lasting integration windows has been demonstrated not only in visual perception (Scharnowski et al., 2009; Mudrik et al., 2011; Akyürek & Wolff, 2016; Marti & Dehaene, 2017; Sergent, 2018), but also in auditory perception (McWalter & McDermott, 2019) and across different sensory modalities (Fiebelkorn et al., 2010; Stiles et al., 2018; Rimsky-Robert et al., 2019).

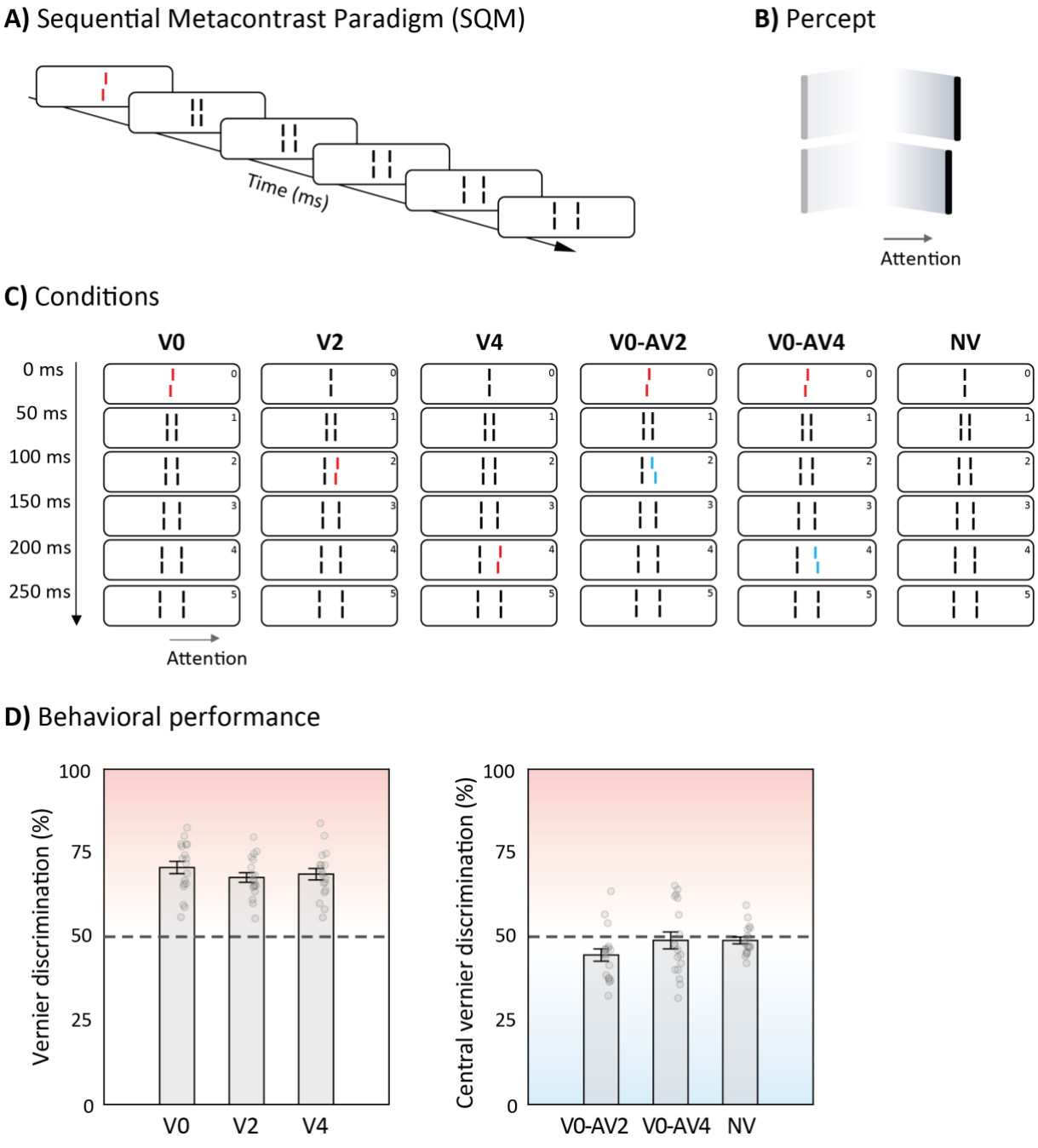

Figure 1. A) The Sequential Metacontrast paradigm (SQM). A central line, here with a left vernier offset, is followed by pairs of flanking lines eliciting a percept of two diverging streams. (B) Observers attend to one stream, in which all offsets are integrated. C) In V conditions, only one vernier is presented, either in the central line (V0), in the second (V2), or in the fourth(V4) flanking line. In V-AV conditions, the central line is offset, and one of the flanking line is offset in the opposite direction (anti-vernier; V0-AV2 or V0-AV4). In the control condition (NV), only straight lines are shown. The red and blue vernier offsets in the figure are for illustration purposes only; in the experiment, all lines were the same color. D) Participants attended to the right stream and were asked to report the perceived offset direction (right/left) of the first presented vernier offset by pressing hand-held push-buttons. In V conditions, participants could accurately report the offset direction. In V-AV conditions, participants could not perceive the individual vernier offsets, and hence performance is at 50%. This indicates that both vernier offsets contribute equally. When no vernier was presented or perceived, participants were guessing. In NV condition, performance is determined by comparing the response to a randomly chosen offset.

In this study, we used EEG decoding to investigate the neural mechanisms involved in both the unconscious integration of vernier offsets and the subsequent emergence of a conscious percept. Our approach was guided by the following rationale: in the SQM, regardless of the number and spatio-temporal locations of the verniers, all offsets are *integrated unconsciously*, and only a single offset is *consciously perceived*—the weighted outcome of all unconsciously processed verniers. Neural activity encoding information about the number or location of individual offsets should therefore reflect unconscious processing, whereas neural activity encoding the integrated outcome should reflect processes linked to the *content* of the conscious percept.

Results

Unconscious feature integration within the SQM stream

In the SQM, participants consistently integrate the vernier offsets with all the lines presented in the attended stream, regardless of how many offsets are present, i.e., individual elements cannot be perceived separately (Drissi-Daoudi et al., 2019; Vogelsang et al., 2023).

For example, in the conditions with only a single vernier in the stream (V conditions; Figure 1A and 1C), the offset was perceived as extending across the entire sequence of lines (Otto, 2006; Otto et al., 2010; Figure 1B), and offset discrimination performance was above the 50% chance-level (Figure 1D, left panel). This effect was consistent regardless of where the offset appeared in the stream; whether the offset occurred in the central line or in the second or fourth flanking lines, the mean accuracy remained high (70% ± 7%). Paired t-tests comparing each of these V conditions with a no vernier (NV) control condition resulted all in significant differences (all $p < .001$, Cohen's $d' > 3.3$; Figure 1D, left panel).

In contrast, when two opposite vernier offsets (a vernier and an anti-vernier) were included in the stream (V-AV condition, Figure 1C), the offsets were mandatorily integrated. Mean accuracy in reporting the first offset was 47% ± 9%, comparable to the NV condition (paired t-tests between the V-AV and NV conditions: all $p > .05$; Figure 1D, right panel). Thus, conscious perception does not depend on the location and number of offsets in the stream, as there is no conscious percept of the individual elements.

Neural representations preserve the chronology of events in the SQM stream

We first aimed to decode neural activity related to the processing of vernier offsets. To this end, we applied Linear Discriminant Analysis (LDA) to EEG activity patterns to decode the presence and location of vernier offsets across the stream.

We ran separate LDA classifiers using a temporal generalization approach (i.e., classifiers were trained on data from each time point and tested across all other time points; see Methods) to discriminate between trials with no offset (NV condition) and trials with a single vernier offset presented at different spatio-temporal locations within the stream (V0: 0 ms, V2: 100 ms, V4: 200 ms, Figure 1C). The classifiers successfully discriminated the presence of a vernier offset in all V conditions (Area Under the Curve, AUC > 0.5, one-tailed cluster-based permutation test, $p < .05$; Figures 2A and 2B). The resulting patterns were similar across conditions, with decoders generalizing only over short time windows, as indicated by higher decoder performance when both training and testing occurred at the same time points (i.e., the diagonal elements of the temporal generalization matrices).

Crucially, the decoding latencies revealed systematic delays that corresponded to the actual location of the vernier offset in the stream—decoding was successful at 240 ms for V0 vs. NV, at 330 ms for V2 vs. NV, and at 370 ms for V4 vs. NV (Figure 2B). Hence, although participants perceived the offset as present along the entire stream, the presence of an offset was decoded only around 200 ms (170–240 ms) after its physical onset, with a slightly decreasing delay when the vernier was presented later in the stream.

This result was further supported by cross-condition decoding, where we trained a classifier on discriminating V2 vs. NV or V4 vs. NV and tested it on V0 vs. NV. This revealed shared neural representations of the single vernier across conditions but shifted along the diagonal in the cross-condition temporal generalization matrix (Figure 2C). That is, a decoder trained to detect the vernier in the V2 or V4 condition successfully decoded it in V0 (AUC > 0.5, one-tailed cluster-based permutation test, $p < .05$), but with earlier onsets of approximately 100 and 200 ms, respectively, corresponding to the actual latencies between conditions.

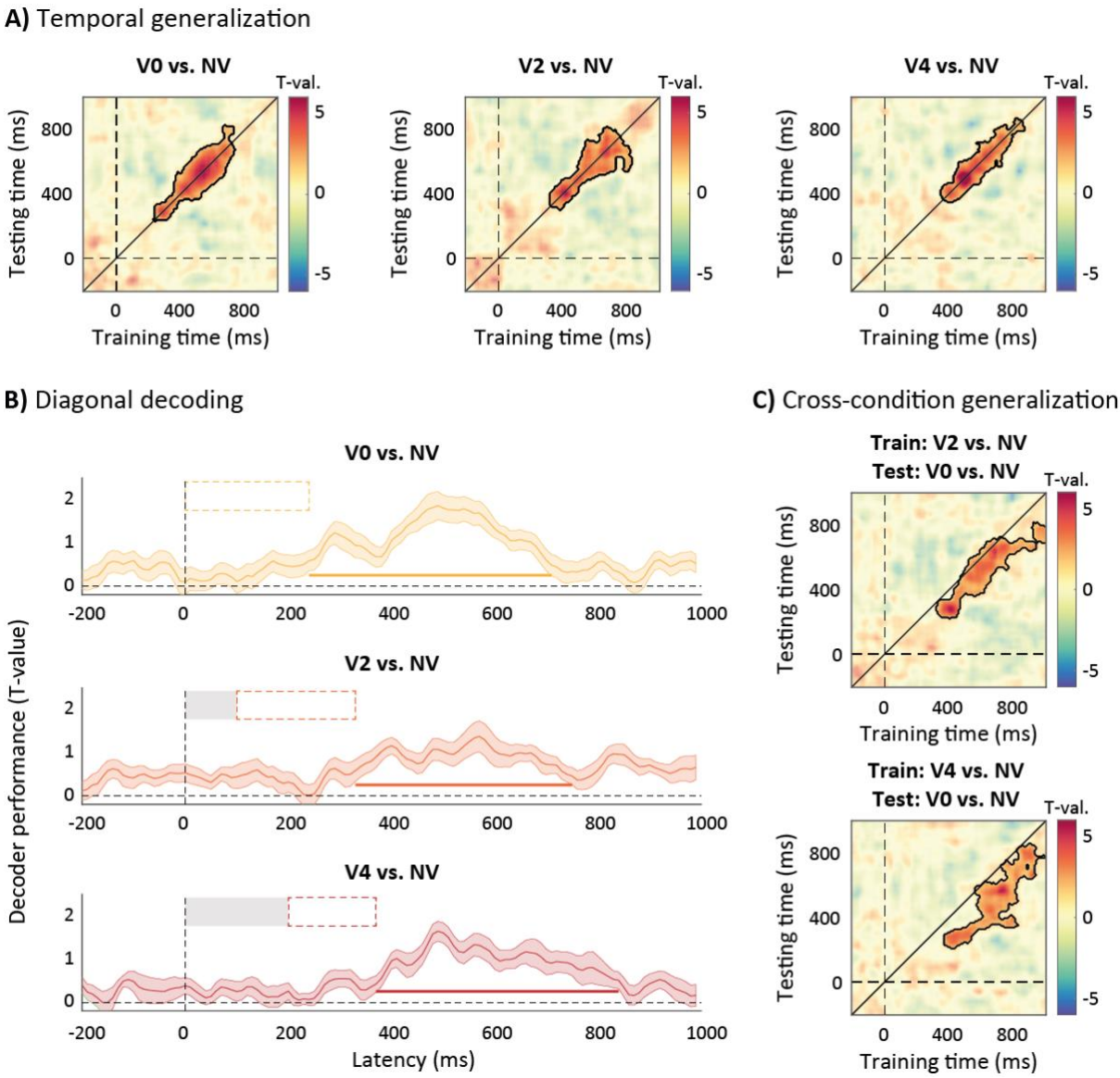

Figure 2. Linear discriminant analysis (LDA) with temporal and cross-condition generalization to decode conditions with one vernier and no vernier. A) Temporal generalization matrices, obtained by training a classifier on data at every time point and testing it at all other time points, showing that classifiers can successfully discriminate between the conditions (V0, V2, and V4 vs. NV). Significant clusters are highlighted (AUC > 0.5, one-tailed cluster-based permutation test, $p < .05$). B) Diagonal elements of the temporal generalization matrices, representing decoding results when training and testing at the same time point (group average AUC and SEM). Significant time windows are highlighted by the horizontal lines at the bottom. Temporal delays in the decoding results, relative to the actual onset of the vernier in the stream, are indicated by the dashed rectangles. C) Cross-condition generalization matrices showing that classifiers trained with V2 or V4 vs. NV successfully discriminate V0 vs. NV but with earlier onsets corresponding to the effective stimulus delay between V0 and V2 (i.e., 100 ms later) and V4 (i.e., 200 ms later). Significant clusters are highlighted (AUC > 0.5, one-tailed cluster-based permutation test, $p < .05$).

Decoding the conditions with a single vernier against the condition with no vernier was significant in windows ranging from 240 to 710 ms in V0 vs. NV, 330 to 750 ms in V2 vs. NV, and 370 to 840 ms in V4 vs. NV). In these time windows, we found two distinct EEG activation patterns—i.e., topographies of EEG activity associated with the decoder results (see Methods

and Figure 3A). These scalp patterns and their transitions were consistent across participants (Figure 3A, bottom row, Cohen's *d* of the scalp activation patterns at the group level).

The first topography displayed stronger activation over occipital electrodes, with increasing duration as the vernier offset occurred later in the stream (Figure 3B). The second topography, which showed increased activation over parietal electrode sites, had a shorter duration when the vernier offset occurred later (Figure 3B). The time course of these topographies, estimated by back-projecting activation patterns onto the original EEG time series, revealed a clear transition between the two patterns, with evident temporal shifts across conditions (i.e., the transition occurred around 360 ms in V0 vs. NV, 460 ms in V2 vs. NV, and 570 ms in V4 vs. NV; Figure 3C).

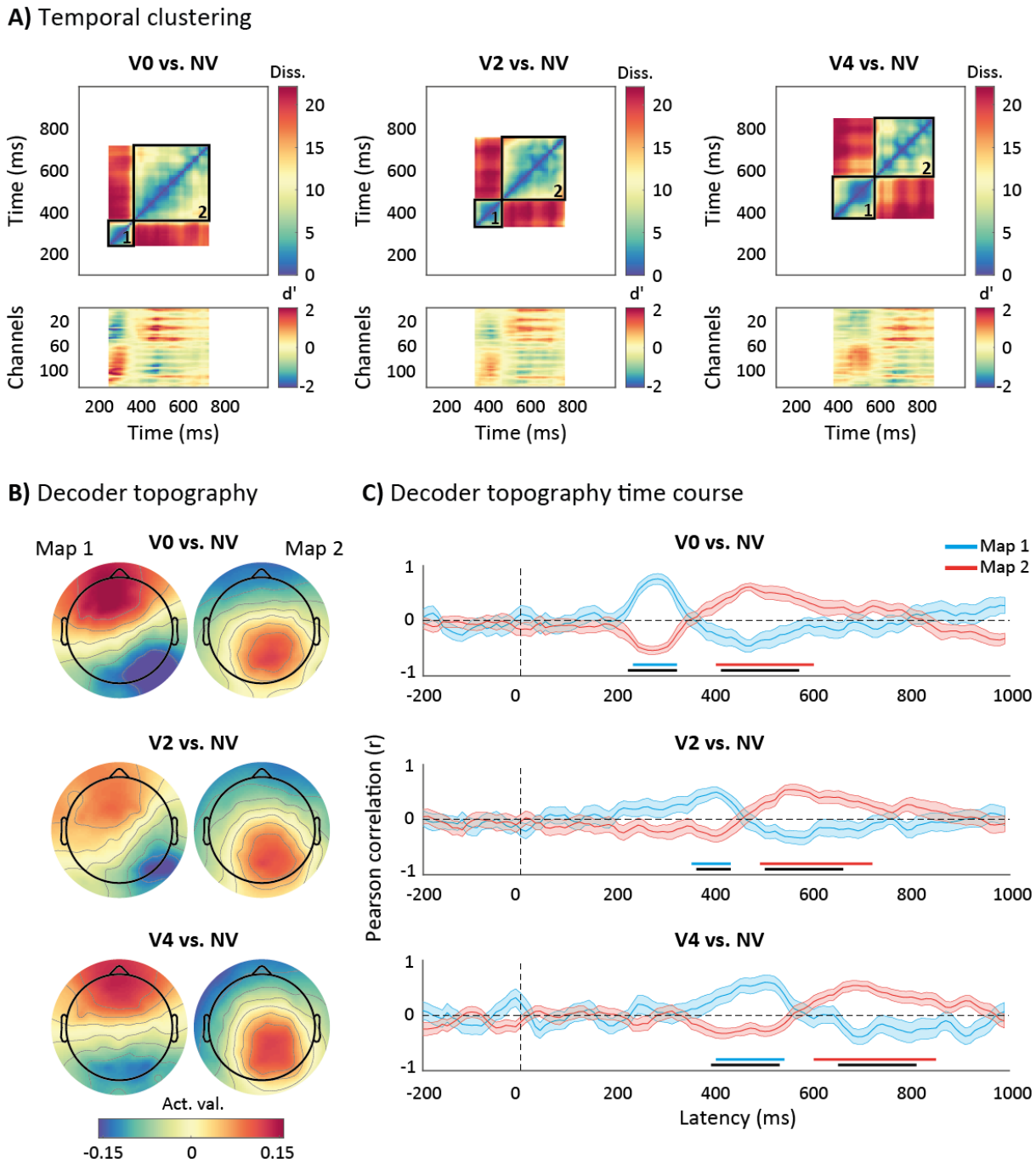

Figure 3. EEG activation patterns contributing to decoding conditions with one vernier and no vernier. A) Analysis of dissimilarity matrices between the EEG activation patterns extracted from significant time points (diagonal elements of the temporal generalization matrices for V0, V2, or V4 vs. NV; see Figure 2B) reveals a clear transition between two main activation patterns (outlined by black squares) for each decoding analysis (upper row). These activations patterns were consistently expressed across participants, as indicated by the large effect sizes (Cohen's *d*) for the difference between each activation pattern and zero, calculated for each electrode and time point (bottom row). B) Decoder topographies, averaged across participants, are derived from the two main activations patterns identified with the analysis of dissimilarity matrices. Each decoding analysis shows similar topographical maps but with variations in their transition dynamics. C) Temporal correlations between the two identified topographies and the back-projected time course of EEG activation patterns for each decoding analysis. Blue and red lines represent the first and second topographies, respectively, and the shaded areas indicate SEM. Significant correlations are also highlighted in blue for the first map or in red for the second (Pearson's $r > 0$, one-tailed cluster-based permutation test, $p < .05$), while significant differences between the two time courses are shown in black (two-tailed cluster-based permutation test, $p < .05$).

Neural correlates of unconscious processing

Up to this point, we have focused on conditions featuring a single vernier, whose offset is consciously perceived throughout the entire stream. Even though the location of the vernier was not consciously perceived, it could still be decoded via two distinct EEG topographies. Next, we analyzed conditions involving two opposite vernier offsets, separated by varying intervals (V0-AV2: 50 ms, V0-AV4: 150 ms; Figure 1C), using LDA to distinguish these conditions from a condition featuring only straight lines (NV).

In the V-AV conditions, behavioral performance was around 50%, indicating mandatory integration of the two opposite offsets (Figure 1D). As previously suggested (Menétrey et al., 2023), in the V-AV condition one of the two vernier offsets might still dominate the integration, with trial-by-trial fluctuations in pre-stimulus EEG activity determining whether the first or second offset prevails. Thus, although these fluctuations result in overall chance-level performance, perception in the V-AV condition may still correspond to a weak, integrated offset, differing from the perception of a straight moving line in the NV condition.

Consistent with this, the decoder successfully discriminated V0-AV2 or V0-AV4 trials from NV trials (AUC > 0.5, one-tailed cluster-based permutation test, $p < .05$; Figure 4A). In both analyses, the significant decoding windows (170-1000 ms; Figure 4B) exhibited a similar sequence of EEG activation patterns (Figure 4C), with topographies (Figure 4D) closely resembling those observed in the V0 vs. NV decoding analysis (Figure 3B). Similarly, the significant decoding onsets and the transition dynamics around 370 ms (Figures 4B and 4E) closely mirrored those found in V0 vs. NV conditions (Figures 2B and 3C for comparison). Thus, EEG activation patterns distinguished the presence of two offsets from no offsets, even though the individual offsets were integrated and not perceived separately.

Furthermore, cross-condition decoding revealed that a decoder trained to detect the vernier in the V0 condition (vs. NV) still successfully decoded, with similar onset and temporal dynamics, V0-AV2 or V0-AV4 conditions from NV condition (AUC > 0.5, one-tailed cluster-based permutation test, $p < .05$, Figure 4F), confirming a shared neural representation of a single vernier even in conditions with two opposite vernier offsets.

The key question that follows is whether the two EEG activation patterns observed reflect the conscious perception of a single vernier throughout the stream, or instead capture successive stages in which each individual vernier is first processed unconsciously and later integrated into a unified percept.

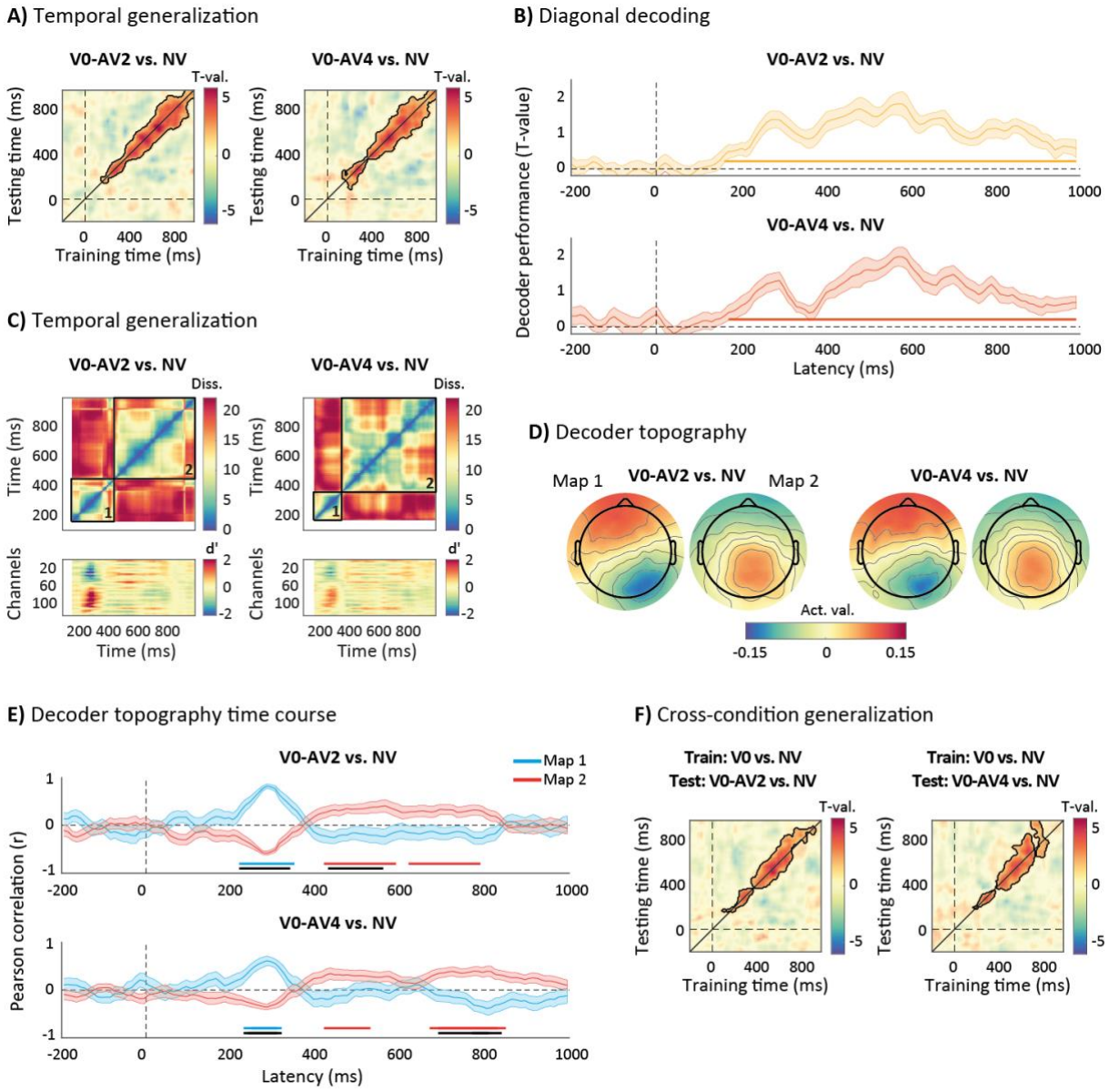

Figure 4. Linear discriminant analysis (LDA) with temporal and cross-condition generalization to decode conditions with two opposite verniers and no vernier. A) Temporal generalization matrices showing that classifiers successfully discriminate the conditions (V0-AV2 or V0-AV4 vs. NV). Significant clusters are highlighted (AUC > 0.5, one-tailed cluster-based permutation test, $p < .05$). B) Diagonal elements of the temporal generalization matrices for V0-AV2 or V0-AV4 vs. NV, representing decoding results when training and testing at the same time point (group average AUC and SEM). Significant time windows are highlighted by the horizontal lines at the bottom. C) Analysis of dissimilarity matrices between the EEG activation patterns extracted from significant time points reveals a clear transition between two main activation patterns (outlined by black squares) for each decoding analysis (upper row). These activations patterns were consistently expressed across participants, as indicated by the large effect sizes (Cohen's *d*) for the difference between each activation pattern and zero, calculated for each electrode and time point (bottom row). D) Decoder topographies, averaged across participants, are derived from the two main activation patterns identified with the analysis of dissimilarity matrices. Each decoding analysis shows similar topographical maps and transition dynamics. E) Temporal correlation between the two identified topographies and the back-projected time course of EEG activation patterns for each decoding analysis. Blue and red lines represent the first and second topographies, respectively, and the shaded areas indicate SEM. Significant correlations are also highlighted in blue for the first map or in red for the second (Pearson's $r > 0$, one-tailed cluster-based permutation test, $p < .05$), while significant differences between the two time courses are shown in black (two-tailed cluster-based permutation test, $p < .05$). F) Cross-condition generalization matrices showing that classifiers trained with V0 vs. NV successfully discriminate V0-AV2 or V0-AV4 vs. NV with similar onset. Significant clusters are highlighted (AUC above 0.5, one-tailed cluster-based permutation test, $p < .05$).

To address this question, we tested whether the two V-AV conditions, where the second vernier occurred at different times (V0-AV2 vs. V0-AV4), could be decoded from V0 trials, where only a single vernier was shown and consciously perceived. Significant decoding in this comparison would indicate neural correlates of the second vernier offset that was processed unconsciously and integrated with the first vernier. Consistent with this prediction, we found significant decoding for both comparisons (AUC > 0.5, one-tailed cluster-based permutation test, $p < .05$; Figure 5A). The decoding windows (from 300 ms for V0-AV2 vs. V0, and from 340 ms for V0-AV4 vs. V0) were compatible with the latencies observed when decoding conditions with a single vernier presented later in the stream (V2 or V4 vs NV, Figure 2B), supporting the idea that neural representations of the second vernier persisted, even though this offset was not consciously perceived as a separate event.

Moreover, the two V-AV conditions, despite yielding identical conscious percepts, were reliably discriminated from each other (AUC > 0.5, one-tailed cluster-based permutation test, $p < .05$; Figure 5A). That is, EEG activation patterns contained information about the different location of the second vernier across the two conditions, which was decodable starting from 420 ms onward, even though participants neither consciously perceived nor could report this second vernier.

The average activation pattern contributing to these decoding results (Figure 5B) resembled the first topography identified when contrasting conditions with one or two offsets from the condition without any offset (Figures 3B and 4D). This topography dominated and remained stable throughout the significant decoding windows and across the three analyses (V0 vs. V-AV and V0-AV2 vs. V0-AV4; see Figure 5B, effect size plots). To further validate this finding, we correlated the activation patterns obtained here with the two prototypical topographies derived from averaging across all V or V-AV vs. NV decoding analyses (Figures 3B and 4D; see Methods). The results confirmed the dominant contribution of the first prototypical topography (Figure 5C), temporally aligned with the onset of the second vernier.

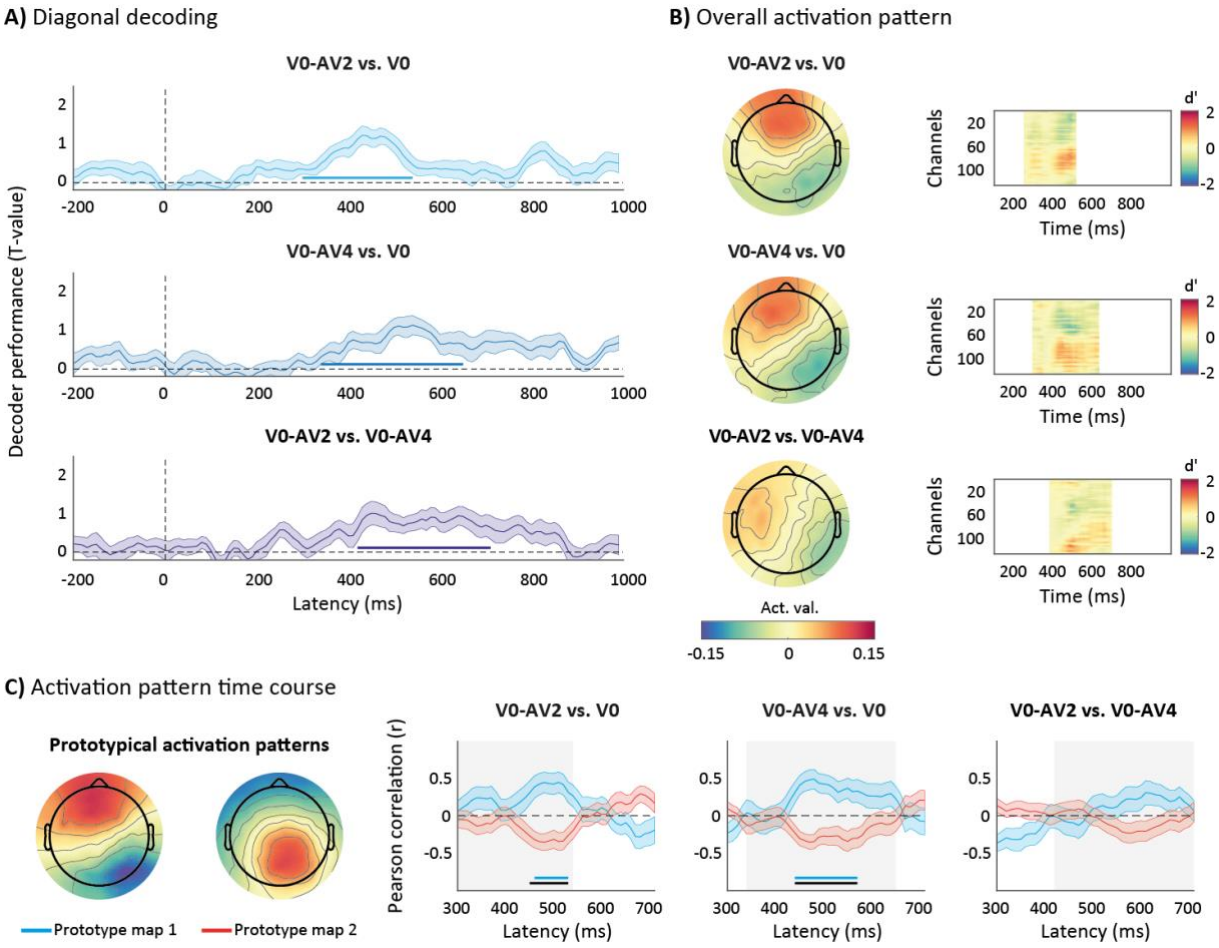

Figure 5. Linear discriminant analysis (LDA) with temporal generalization to decode conditions with one and two verniers and between conditions with two verniers. A) Diagonal elements of the temporal generalization matrices, representing decoding results when training and testing at the same time point (group average AUC and SEM). Significant time windows are highlighted by the horizontal lines at the bottom, showing that classifiers successfully discriminate the conditions (V0-AV2 or V0-AV4 vs. V0, and V0-AV2 vs. V0-AV4; AUC > 0.5, one-tailed cluster-based permutation test, $p < .05$). B) The decoder topographies, averaged across participants, are derived from the averaged activation pattern over the entire significant window of each decoding analysis. These activation patterns were consistently expressed across participants and over time, as reflected by the effect sizes (Cohen's d) computed for the difference between each activation pattern and zero at each electrode and time point. C) Prototypical activation patterns (left side), corresponding to the average of the two distinct activation patterns identified via dissimilarity matrix analysis for all V or V-AV vs. NV contrasts (see Figures 3B and 4D), were temporally correlated with the activation patterns found in each decoding window (right side; the gray area highlights the significant window found in 5A). Blue and red lines represent the first and second topographies, respectively, and the shaded areas indicate SEM. Significant correlations are also highlighted in blue for the first map or in red for the second (Pearson's $r > 0$, one-tailed cluster-based permutation test, $p < .05$), while significant differences between the two time courses are shown in black (two-tailed cluster-based permutation test, $p < .05$).

Based on these findings, we interpret the first topography as the neural correlate of unconscious processing of the vernier stimuli, occurring prior to the formation of the integrated percept. Conversely, the presence of the second topography when discriminating V-AV from NV trials (Figure 4D) might reflect the content of the final integrated percept. Indeed, the latencies and sequence of topographies in these decoding analyses are similar to those observed in the condition with a single vernier presented in the central line (V0; Figure 3B), supporting

290 the view that, in V-AV conditions, participants still perceive an offset in the stream, although a
291 weaker one (see also Supplementary Figure S1 for additional cross-condition generalization
292 evidence between V and V-AV conditions, as a function of whether the first or second vernier
293 dominated the reported percept).
294
295 *Neural correlates of the integrated percept*
296 To directly assess the involvement of the second topography in conscious processing, we
297 applied LDA to decode correct vs. incorrect reports of the offset direction in the conditions
298 featuring only a single vernier (V conditions). As shown in Figure 6, the classifiers successfully
299 decoded behavioral performance in all single-vernier conditions (Figure 6A; AUC > 0.5, one-
300 tailed cluster-based permutation test, $p < .05$). However, significant decoding emerged at later
301 latencies—480 ms for V0, 460 ms for V2, and 570 ms for V4—compared to the earlier latencies
302 observed when decoding V or V-AV conditions against the NV condition.
303 In addition, the topographies obtained by averaging the main activation patterns across
304 the entire significant decoding window (Figure 6B) were clearly distinct from those identified
305 in the previous decoding analyses (V0 vs. V-AV and V0-AV2 vs. V0-AV4; Figure 5B).
306 Correlations with prototypical activation patterns confirmed that decoding of the correctly
307 reported direction was driven by a single EEG activation pattern (Figure 6C), which in this case
308 aligned with the second topography identified when decoding conditions with one or two offsets
309 from trials without any offset (Figures 3B and 4D). This topography exhibited latency shifts as
310 a function of the vernier's temporal position within the stream and appeared to persist longer
311 when the vernier occurred later in time (see also Supplementary Figure S1 for analogous effects
312 in V–AV conditions, depending on whether the first or second vernier dominated the integrated
313 percept).
314 Thus, the later decoding of correct versus incorrect responses—compared to the earlier
315 decoding reflecting differences in the location or number of verniers in the stream—indicates
316 that this centro-parietal topography reflects a neural correlate of a later stage, involving
317 processes associated with the consciously perceived vernier offset, rather than the initial stage
318 of unconscious integration.

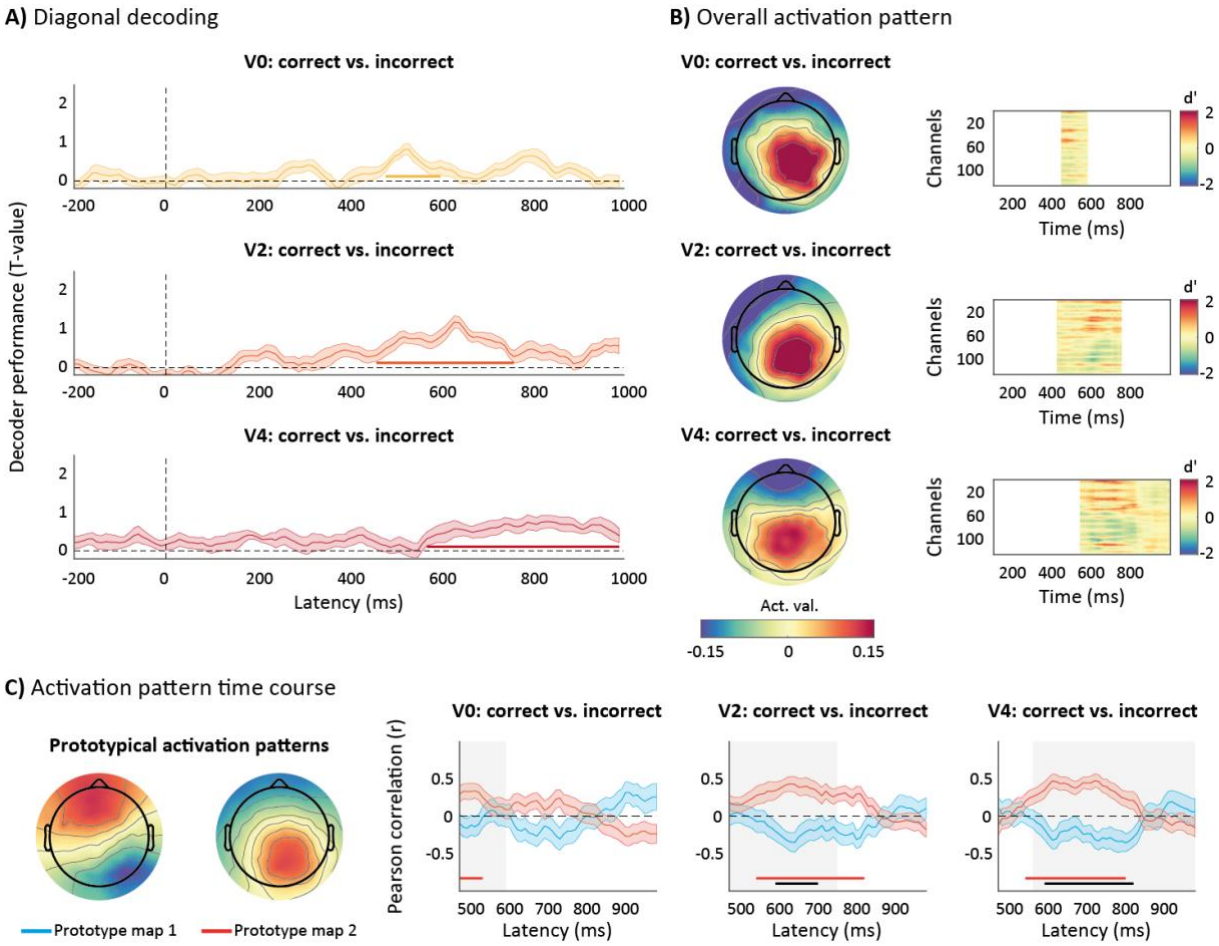

Figure 6. Linear discriminant analysis (LDA) with temporal generalization to decode correct and incorrect reports in conditions with one vernier. A) Diagonal elements of the temporal generalization matrices, representing decoding results when training and testing at the same time point (group average AUC and SEM). Significant time windows are highlighted by the horizontal lines at the bottom, showing that classifiers successfully discriminate correct from incorrect offset reports in all V conditions (V0, V2 or V4; AUC > 0.5, one-tailed cluster-based permutation test, $p < .05$). B) The decoder topographies, averaged across participants, are derived from the averaged activation pattern over the entire significant window of each decoding analysis. These activation patterns were consistently expressed across participants and over time, as reflected by the effect sizes (Cohen's d) computed for the difference between each activation pattern and zero at each electrode and time point. C) Prototypical activation patterns (left side), corresponding to the average of the two distinct activation patterns identified via dissimilarity matrix analysis for all V or V-AV vs. NV contrasts (see Figures 3B and 4D), were temporally correlated with the activation patterns found in each decoding window (right side; the gray area highlights the significant window found in 6A). Blue and red lines represent the first and second topographies, respectively, and the shaded areas indicate SEM. Significant correlations are also highlighted in blue for the first map or in red for the second (Pearson's $r > 0$, one-tailed cluster-based permutation test, $p < .05$), while significant differences between the two time courses are shown in black (two-tailed cluster-based permutation test, $p < .05$).

Discussion

Previous studies have proposed that in the SQM, and in related postdictive phenomena, conscious perception is preceded by a period of unconscious processing (Choi & Scholl, 2006; Wu et al., 2009; Elliott & Giersch, 2016; Sergent, 2018; Keuninckx & Cleeremans, 2021; Herzog et al., 2016, 2020). In the SQM, a sequence of lines and vernier offsets is mandatorily and unconsciously integrated for up to 450 milliseconds before a conscious percept emerges (Drissi-Daoudi et al., 2019; Vogelsang et al., 2023). Here, we used time-resolved decoding analysis to identify EEG markers of this unconscious integration stage and to track the transition toward the final integrated percept.

We found that each vernier in the stream could be decoded from EEG activity time-locked to the moment it was shown, with decoding emerging around 200 ms later (Figure 2). This was the case even though the consciously perceived vernier offset does not depend on the number or specific spatio-temporal location of the verniers within the SQM stream. Importantly, individual verniers remained decodable even when two opposite verniers were presented and their offsets were obligatorily integrated (Figure 4). These results indicate that, even when individual vernier offsets are not consciously perceived, their presence and temporal position can still be inferred from neural activity.

The decoding of individual vernier offsets was driven predominantly by occipital activity (see Figures 3 and 4), with a topography resembling the N170/VAN ERP component. Although this component has often been proposed as an early correlate of conscious perception (Ojanen et al., 2003; Koivisto & Revonsuo, 2010; Railo et al., 2011; Dembski et al., 2021), several studies have also reported it in response to unseen stimuli (Sterzer et al., 2009; Harris et al., 2013; Cohen et al., 2024). Our results suggest that the N170/VAN may reflect an unconscious rather than a conscious processing stage, consistent with studies linking this component to the unconscious accumulation and integration of visual information (Fahrenfort et al., 2017; Noorman et al., 2025).

The N170/VAN-like component was also observed when decoding between conditions involving one or two verniers (Figure 5), even though both conditions produced the same integrated percept—namely, a single vernier offset perceived throughout the stream. Because these conditions differed in the location or number of physical offsets, this finding suggests that the topography reflects differences in the sequence of unconsciously processed events, supporting its role as a neural correlate of unconscious integration. It is also worth noting that this topography was right-lateralized (ipsilateral to the stimulus). The origin of this

lateralization remains unclear, but one possibility is that the right hemisphere dominates processing of motion-related signals from both visual hemifields (Chiappini et al., 2022; Pitcher, 2022), or that it is more generally specialized for visuo-spatial processing (Corballis, 2003).

Following this first topography, we identified a distinct centro-parietal topography (see Figures 3 and 4). This second topography contributed to decoding conditions with one or more verniers against the condition with no vernier, but it did not emerge when decoding between conditions containing one versus two verniers. This suggests that it carries information about the integrated percept, regardless of whether it arises from a single vernier or from the integration of two. Consistent with this interpretation, a similar centro-parietal topography was observed when decoding correct versus incorrect behavioral reports of the offset in conditions with a single vernier (see Figure 6). This topography emerged after approximately 450 ms and persisted for several hundred milliseconds, resembling the P300 ERP component.

The P300 is often described as a neural correlate of conscious access (Sergent et al., 2005; Del Cul et al., 2007; Kouider et al., 2013; Weaver et al., 2019; Ye et al., 2019; Noorman et al., 2025) and has been linked to late-access models of consciousness, where conscious perception arises from higher-order, distributed or recurrent neural processes (Baars, 2002; Dehaene et al., 2006; Lau, 2007; Dehaene & Changeux, 2011; Naccache, 2018; Seth & Bayne, 2022). However, recent studies suggest that, rather than reflecting the neural correlates of conscious perception, the P300-like component may index post-perceptual processing stages, such as decision-making and response-related activity, because it is often absent in no-report paradigms or for task-irrelevant but consciously perceived stimuli (Pitts et al., 2014; Schlossmacher et al., 2020; Cohen et al., 2020; Sergent et al., 2021). In our task, a direct motor contribution can be ruled out, as responses occurred much later, around 900 ms, but a post-perceptual origin remains possible.

We suggest that the critical shift from unconscious processing to the unified integrated percept is not reflected in the P300-like component itself, but rather in the transition from the first to the second topography. This interpretation is further supported by the close temporal alignment between this transition (Figures 3 and 4) and the window of unconscious integration previously estimated from behavioral measures (~330 and 450 ms; Drissi-Daoudi et al., 2019; Vogelsang et al., 2023).

Thus, our results support the existence of long-lasting unconscious processing windows, which have been reported in other postdictive paradigms beyond the SQM (Sergent et al., 2013;

Akyürek & Wolff, 2016; Thibault et al., 2016; Xia et al., 2016; Sun et al., 2017), and even with briefly presented stimuli. For example, when a 30 ms vernier is followed by a 30 ms anti-vernier, participants perceive a single integrated vernier without any percept of apparent motion (Scharnowski et al., 2009). Yet, transcranial magnetic stimulation (TMS) can alter this integrated percept up to 360 ms after stimulus onset, shifting dominance toward one of the two initial verniers depending on the timing of the TMS pulse (Scharnowski et al., 2009). These findings collectively support the idea that unconscious integration can persist well beyond the physical presence of the stimulus (see also Pilz et al., 2013 for additional evidence using visual features other than vernier offsets). Although the unconscious integration window appears relatively long in the SQM, consistent with the fact that individual vernier offsets are not perceived as separate events, it remains possible that in other tasks this window is shorter, allowing conscious perception to emerge earlier.

Indeed, our results show that the temporal dynamics of unconscious and conscious processing stages are not fixed, and may vary even within the same paradigm. For example, when decoding conditions with a single vernier against conditions without any vernier (Figures 2 and 3), the latency between the vernier presentation and the onset of significant decoding decreased when the vernier appeared later in the stream (from 240 ms in V0 vs NV to 170 ms in V4 vs NV; Figure 2B). In these conditions, the first topography persisted for a longer duration, whereas the second was shortened (Figure 3A). Moreover, the onset and duration of the second topography appeared to depend on the location of the vernier dominating the unconscious integration process (Figure 6A; Supplementary Figure S1). Although the exact nature of these non-linearities remain unclear, these results indicate that the temporal dynamics of unconscious and conscious processing stages are flexible and may be influenced by subtle details of the stimulus sequence, in contrast to standard ERP analyses, which often treat processing latencies as fixed.

In general, the fact that neural activity is time-locked to a stimulus (see Figure 2) does not imply that conscious perception occurs at that moment (the 'vehicle problem', Dennett & Kinsbourne, 1992; Herzog et al., 2020; Dainton, 2023; White, 2023), just as a neuron that encodes "red" is not itself red. This contrasts with theories assuming a close mapping between stimulus timing and the moment of perception (e.g., the 'brain-time' view, Holcombe, 2014) and implies that neither the transition between the two topographies nor the duration of the second topography necessarily reflects neural events involved in conscious perception itself. Instead, these neural signatures may act as precursors to consciousness or, as mentioned, reflect

post-perceptual processes operating on the content of the percept. Nevertheless, this transition marks the shift from the unconscious encoding of the physical, retinotopic properties of the vernier offset—which are not perceived consciously—to the integrated representation of the stream, which forms the basis of conscious perception in the SQM. Thus, while the exact timing of conscious perception cannot be inferred directly from these topographies, they reveal the sequential neural processes that enable the emergence of a coherent percept.

In line with this, throughout the manuscript we use the terms conscious processing and conscious perception to refer to the stage in which an integrated percept of the entire SQM stream has emerged. These terms are used in contrast to the unconscious processing of individual offsets in the SQM, which participants cannot perceive individually. We must clarify, however, that by these terms we do not intend to imply or distinguish between phenomenal consciousness (i.e., the felt quality of a conscious mental state) and access consciousness (i.e., the functions enabled by conscious processing, such as behavioral reports), as our paradigm is not designed to address this distinction (Block, 2007; Michel & Doerig, 2022). As mentioned, we use the terms broadly to include also post-perceptual, decision-making processes associated with the emergence of an integrated percept.

The presence of two distinct topographies, and their temporal dynamics, is compatible with a recently proposed two-stage model of perception in which a prolonged period of unconscious processing precedes the emergence of a unified conscious percept (Herzog et al., 2016, 2020). In this framework, the first stage involves the precise encoding of each vernier offset and its temporal position, with this information maintained in a high-capacity buffer where integration operates unconsciously. This stage aligns with the independent neural encoding of individual verniers observed in our decoding results and reflected in the first topography (Figures 3, 4 and 5). In the second stage, the unconscious processing window enables a form of sense-making: the brain resolves the buffered information into the most coherent percept over the preceding hundreds of milliseconds. At the end of this stage, the buffered information collapses into a conscious percept that reflects the integrated structure of the sequence. This transition, and the emergence of a unitary percept, align with the decoding results associated with the second topography (Figures 3, 4 and 6). Overall, these sequential stages are consistent with discrete retentional models in which perception is momentary but temporally rich, delayed relative to stimulus onset, yet encoding quantitative details such as duration, speed, and direction (Herzog et al., 2016). Such dynamics do not contradict the existence of “fast” perceptual phenomena such as rapid visual detection (Thorpe et al., 1996)

or the effects of masking (Breitmeyer & Öğmen, 2007). Detection, object recognition, and even action can unfold during unconscious processing without immediately giving rise to conscious awareness (Dehaene et al., 1998; Mitroff & Scholl, 2005; Van Gaal et al., 2012; but see also Biderman & Mudrik, 2018; Mudrik & Deouell, 2022).

In sum, our findings support the presence of sequential processing stages in the SQM and related phenomena, with an extended period of unconscious visual processing followed by a transition to a unified, conscious percept. This has direct relevance for efforts to identify the neural correlates of conscious perception, as most theoretical frameworks, except for the global neuronal workspace theory (Dehaene et al., 2006; Dehaene & Changeux, 2011), do not explicitly separate unconscious from conscious processing stages (for reviews, see Aru et al., 2012; Storm et al., 2017). Acknowledging this two-stage structure may therefore provide a useful foundation for future research on the temporal organization of conscious and unconscious visual processing.

Materials and Methods

Participants

A total of 18 naive, healthy participants (9 females; age range: 18-23 years old) were recruited for the experiment. Participants had normal or corrected to normal vision, as assessed through the Freiburg acuity test (threshold for inclusion: >1; Bach, 1996). All participants signed informed consent before the experiment and received monetary compensation upon its completion. The experiment was conducted with the approval of the local ethics commission (Commission cantonale d'éthique de la recherche sur l'être humain, Canton of Vaud, Switzerland; protocol number: 2021-02270; title: Fundamental aspects of object recognition) and in accordance with the Declaration of Helsinki (except for pre-registration).

Apparatus

The stimuli were presented on an ASUS VG248QE LCD monitor with a resolution of 1920 x 1080 pixels, a screen size of 24.5 inches, and a refresh rate of 144 Hz. MATLAB R2022b (MathWorks Inc., Natick, MA, USA) along with Psychtoolbox (Brainard, 1997) was used to generate the stimuli. During the experiment, participants were seated at a distance of 1.5 meters from the screen in a dimly lit room. The stimuli appeared as white with a luminance of 100 cd/m², displayed against a uniform black background with a luminance of 1 cd/m².

Stimuli and experimental procedure

We used the sequential metacontrast paradigm (SQM), introduced in Otto et al. (2006), which creates the perception of two motion streams diverging from the center (Figures 1A and 1B). The sequence always began with the presentation of a central vertical line, comprising an upper and a lower segment (the length of each segment is 26.6 arcmin, with a width of 1.2 arcmin) separated by a small vertical gap (2.5 arcmin). Next, pairs of flanking lines appeared progressively further away from the center (horizontal separation between each line is 5 arcmin). The central line and all subsequent pairs of lines were presented for 27.8 ms each, with an interstimulus interval (ISI) of 20.8 ms separating each presentation. The entire stimulus sequence consisted of one central and 5 flanking lines, lasting a total duration of 270.8 ms (Figure 1A).

Participants were instructed to always covertly attend to the right stream. In a randomized order, 6 different conditions were presented (Figure 1C): In the *no vernier* control condition (NV), all lines were straight. In three experimental conditions, one line of the attended

stream was offset, with the lower segment shifted either towards the right or the left relative to the upper segment (referred to as a *vernier offset* or V). In these conditions, the vernier offset was presented either in the first central line (V0 condition), in the second flanker line (V2 condition; 100 ms after stimulus onset) or in the fourth flanker line (V4 condition; 200 ms after stimulus onset). In the two last conditions, the central line always had a vernier offset, while another line in the right stream was offset in the opposite direction (referred to as an *anti-vernier* or AV). In these conditions, the opposite vernier was presented either in the second flanker line (V0-AV2 condition) or in the fourth flanker line (V0-AV4 condition).

In all conditions, participants were asked to indicate whether they perceived a left or right offset along the stream (Figure 1B), even when no vernier was presented (usually observers perceive the offset at the last line, even though the line was always straight). Observers were informed that one or two verniers could be presented in the stream and were instructed to report the first one in case they perceived both.

Participants completed a total of 12 blocks, with each block consisting of 96 trials (192 trials per condition, 1152 trials in total). Before each trial, a central fixation point was presented for 250 ms, followed by an inter-stimulus interval of 750 ms. After the SQM presentation, participants had 3 seconds to give their response by clicking one of two hand-held buttons. If no response was made within this time, the trial was discarded and repeated at the end of the block. In order to eliminate potential early responses that occurred before the complete presentation of the stimulus sequence, we also excluded trials with reaction times below 300 ms after SQM onset (average number of discarded trials: 8.3 ± 21.2). The inter-trial interval was set at 1 second.

Offset calibration

Before the experiment proper, the offset sizes (i.e., the horizontal displacement between their upper and lower segments) were determined to achieve comparable performance levels across participants. Streams of straight lines with one single vernier were presented, and a parameter estimation by sequential testing (PEST) procedure (Taylor & Creelman, 1967) was used to adaptively determine offset sizes leading to around 70% to 80% performance. This was performed with a vernier offset separately at the three different locations tested in the main experiment: the central line (V0), the second flanker line (V2), or the fourth flanker line (V4).

Behavioral analysis

Performance was determined as the proportion of responses that matched the direction of the first presented vernier offset (Figure 1D). We compared performance between the NV condition and each V or V-AV conditions by means of paired t-tests. The NV condition served as a baseline condition; in this condition performance was determined by comparing the response (left or right reported offset) to a randomly chosen notional offset (mean accuracy was 49% ± 4%). All statistical comparisons were Bonferroni-Holm corrected for multiple comparisons (bonf_holm()). When the vernier is presented without an anti-vernier, vernier discrimination should be approximately 75%, in line with the calibration performance. Conversely, when an anti-vernier follows the first (central) vernier, the discrimination of this vernier offset should be around 50%, given the integration of the two verniers. Additionally, we anticipated no performance differences related to the specific locations of the verniers and anti-verniers, as they fell within the same integration window (Drissi-Daoudi et al., 2019). Behavioral performance aligned with this expectation (see Results section).

Across the six tested conditions, average reaction times ranged from 885 ms to 920 ms, with no statistically significant difference between conditions (one-way ANOVA, $F(5, 102) = 0.08$, $p = .99$).

EEG recordings and preprocessing

The EEG data were recorded using a Biosemi Active Two system (Biosemi, Amsterdam, the Netherlands) with a total of 128 Ag–AgCl active electrodes, providing comprehensive scalp coverage. The positioning of the cap was adjusted individually to ensure the Cz electrode was equidistant from the inion and nasion, as well as equidistant from each ear. In addition, the electrooculogram (EOG) was recorded with 4 electrodes positioned 1 cm above and below the right eye and 1 cm lateral to the outer canthi. The recording was referenced to the CMS-DRL ground, maintaining the montage potential close to amplifier zero through a feedback loop. The sampling rate during recording was set at 2048 Hz.

For EEG preprocessing, EEGLAB was utilized (version v2021.1; Delorme et al., 2011; Delorme & Makeig, 2004). The EEG data were first downsampled to 250 Hz. To remove linear trends, detrending was applied (de Cheveigné & Arzounian, 2018), followed by a lowpass filter with a cutoff frequency of 40 Hz. The EEG data were then epoched from -1 s to 1.5 s relative to the onset of the SQM. To ensure data quality, a visual inspection was conducted to identify and exclude epochs (pre-selected with *pop_jointprob* function) or channels with significant

noise or artifacts. Then, an ICA decomposition (*pop_runica* function with Picard algorithm; Ablin et al., 2017a, 2017b) was performed, with a temporary interpolation of the removed channels to maintain a consistent 128-channel configuration across all participants. The ICA decomposition also included "fake" vertical and horizontal EOG recordings, computed from the 4 EOG channels (differences between the channels located above and below the right eye, and between the channels located on the lateral side of each eye). The visually identified independent components associated with eye or muscular artifacts (pre-selected with *pop_icflag* function) were subsequently removed. Lastly, a final interpolation of the removed channels was conducted, along with an average reference including only the EEG channels.

In total, 6.8% of the electrodes were interpolated, while 3.2% of the epochs and 9.1% of the independent components were removed during the preprocessing procedure.

EEG analysis

We aimed to investigate whether brain activity reflects unconscious or conscious processing stages by decoding differences in EEG dynamics in two configurations of the SQM: 1) when only a single vernier is presented at different locations within the stream (V conditions), with all these conditions resulting in the same percept (i.e., one perceived vernier); and 2) when two opposing verniers are presented (V-AV conditions), yet there is no conscious percept of the individual offsets as they integrate.

EEG decoding

Linear discriminant analysis (LDA) with temporal or cross-condition generalization was used to investigate neural representations related to different SQM conditions or percepts. We implemented LDA with custom-made functions written in MATLAB, based on the recommended settings for EEG data (Subasi & Ismail Gursoy, 2010; Grootswagers et al., 2017). For each participant, LDA with temporal generalization was conducted with a leave-one-pseudo-trial-out cross-validation routine (500 iterations). In each iteration, 80% of the trials were sampled and combined into pseudo-trials (average of 20 trials) for the two classes, i.e., the SQM conditions, that were decoded. The mean of the training set was removed to both testing and training sets, and classifier weights were estimated using a regularized covariance (Ledoit & Wolf, 2004; Haufe et al., 2014; Kayser et al., 2016). The classifier weights, obtained from the training set for each time point, were applied to predict the classes in the EEG data of the testing set. Performance was evaluated using the area under the curve (AUC). This process

was repeated for each time point (cross-temporal decoding, i.e., each classifier is tested on all time points), ranging from −200 to 1000 ms, with a sliding window of 7 samples corresponding to a resolution of 70 ms (Grootswagers et al., 2017). LDA with cross-condition generalization was performed similarly and with identical parameters, except that the classes used in the training sets differed from those used in the testing sets. For all decoding analyses, EEG data were resampled at 100Hz and z-scored.

We started by examining V conditions, where the presentation of a single vernier in the stream results in a clear perception of an offset. We used LDA with temporal generalization to discriminate between trials from the control condition (NV) and trials from conditions presenting one single vernier (V0, V2, or V4), irrespective of the behavioral responses (i.e., correct or incorrect report of the vernier offset). The classifiers successfully decoded the presence of information regarding the vernier, indicative of either unconscious or conscious processing stages (Figures 2A and 2B). We also showed some cross-condition generalization between V conditions. Using classifiers trained with V2 or V4 vs. NV conditions, we decoded V0 vs. NV conditions (Figure 2C).

Second, we explored the neural representations in the V-AV conditions, where the two opposite verniers integrate with each other. LDA with temporal generalization was used to classify between trials from the NV condition and one of the two conditions presenting two opposite verniers (V0-AV2 or V0-AV4), irrespective of the behavioral responses (i.e., correct or incorrect report of the first vernier offset). If V-AV and NV conditions cannot be discriminated, it might suggest that significant decoding observed with V conditions reflects only neural correlates of a clearly visible vernier offset. In this scenario, the two opposite verniers in the V-AV conditions would cancel each other out, resulting in the percept of a straight line, akin to the NV condition. However, this does not appear to be the case as the decoder successfully discriminated between these conditions (Figure 4A; see also Figure 4F for cross-condition generalization between V and V-AV conditions), indicating instead that one of the two offsets still dominates the integrated percept (for similar evidence, see Menétrey et al., 2023). Despite a conscious percept of an offset in all conditions with one or two opposite verniers, we were nevertheless able to decode between V0 and V0-AV2 or V0-AV4 conditions, as well as between the two V-AV conditions, demonstrating that unconscious processing also contributes to this significant decoding (Figure 5).

Lastly, we conducted an LDA analysis with temporal generalization to decode between correct and incorrect reports of the offset within each condition presenting one vernier (V0, V2,

and V4; Figure 6). This analysis aimed to specifically identify neural correlates that reflect conscious processing. All parameters remained consistent with those listed above, except for the averaging of trials for pseudo-trials, which was adjusted to 4 due to the reduced number of available trials, especially the incorrect trials (comprising only ~30% of the total for each condition).

Statistical evaluation of decoding analyses

For all decoding analyses, either with temporal or cross-condition generalization, the statistical evaluation of the 2D matrices of cross-temporal decoding results (subjects x time x time) employed cluster-based permutation approaches and surrogate analysis, following established methodologies (Nichols & Holmes, 2002; Maris & Oostenveld, 2007; Kayser et al., 2016). Clusters were defined as consecutive time points where the decoding successfully exceeded chance levels (chance = 0.5, paired t-test with $\alpha = 0.05$). The cumulative t-values within each cluster were then compared to the maximum sum derived from surrogate clusters (permutations = 10'000). Time points were considered statistically significant if the probability in the surrogate data was <0.05 for the corresponding clusters.

EEG activation patterns

We estimated activation patterns from the LDA classifiers using the regression-based approach (eq. [8] in Haufe et al., 2014). Briefly, this method applies an ordinary least squares regression to derive a pattern that, when multiplied by the discriminant signal obtained via LDA, best approximates the original EEG data used as input to the decoder (electrode x time points x pseudotrials). This approach yields a 'forward model' that allows for neurophysiologically interpretable patterns, addressing the known issue of non-interpretable decoder weights (Haufe et al., 2014; Grootswagers et al., 2017).

We assessed the temporal dynamics of the activation patterns in the context of each decoding analysis (V0, V2, or V4 vs. NV, Figure 2; V0-AV2 or V0-AV4 vs. NV, Figure 4; V0-AV2 or V0-AV4 vs. V0, V0-AV2 vs. V0-AV4, Figure 5; correct vs. incorrect reports in V0, V2, and V4, Figure 6). For each subject, we extracted the activation patterns over the significant time points.

Across the five initial decoding contrasts (i.e., all V vs. NV and all V-AV vs. NV conditions; see Figures 2 and 4), we first computed time-by-time dissimilarity matrices based on the spatial topographies of decoder activation in order to characterize the temporal structure

of these EEG activation patterns. These activation patterns were then averaged across participants, and the resulting maps were z-scored across electrodes at each time point to control for overall amplitude differences. Next, we calculated pairwise dissimilarities between all time points within the significant decoding window using the Euclidean distance—a standard measure of topographic dissimilarity that quantifies how different two z-scored maps are by summing the squared differences across electrodes.

This procedure yielded a symmetric dissimilarity matrix that reflects the similarity structure of spatial patterns over time. To identify periods during which activation patterns remained relatively stable (i.e., dominated by similar topographies), we transformed this dissimilarity matrix into a graph representation, where each node corresponded to a time point and edges were defined between pairs of time points with dissimilarity values below the median of the entire matrix. This thresholding ensured that only relatively similar patterns were considered connected in the graph.

We then applied the Louvain community detection algorithm (Blondel et al., 2008; Rubinov & Sporns, 2010), a widely used method for detecting modular structure in networks, to this graph. In this context, the algorithm grouped together contiguous time points that shared similar activation topographies, thereby identifying clusters of temporally stable EEG patterns. To mitigate potential instabilities in the clustering due to noise at the single-subject level, this procedure was performed on group-averaged data. Nevertheless, we verified the robustness of the main findings across participants by estimating effect sizes (see below). The data-driven clustering allowed us to define distinct temporal clusters characterized by dominant topographic maps (Figures 3A and 4C), which were used in subsequent analyses.

Topographies of the main activation patterns were then generated by averaging over temporal windows corresponding to the identified clusters (Figures 3B and 4D), revealing two highly consistent spatial topographies. To examine their temporal characteristics and contributions to the overall dynamics, we correlated these spatial patterns with the temporal evolution of EEG activation (back-projected time courses; Figures 3C and 4D). For each time course independently, as well as for the difference between them, clusters were defined as consecutive time points where the correlation significantly exceeded 0 (paired t-test with $\alpha = 0.05$). The cumulative t-values within each cluster were then compared to the maximum sum derived from surrogate clusters (permutations = 10'000). Time points were considered statistically significant if the probability in the surrogate data was < 0.05 for the corresponding clusters. Notably, while the topographies derived from dissimilarity matrices were based on

group-averaged data, the back-projection plots demonstrate the consistency of these maps and their temporal dynamics across individuals.

To further assess the reliability of the distinct maps across participants, we estimated Cohen's *d* for the difference between each activation pattern and zero at the level of individual electrodes and time points (Figures 3A and 4C). The presence of large effect sizes, both in the positive and negative directions, indicated that the observed topographic patterns were robust and consistently expressed across participants.

For the additional decoding contrasts (i.e., V0 vs. V-AV conditions, V0-AV2 vs. V0-AV4 and correct vs. incorrect reports in V conditions; see Figures 5 and 6), topographies of the main activation patterns were generated by averaging over the entire significant decoding window (Figures 5B and 6B). In addition, we averaged the two maps identified across all decoding results between NV vs. V or V-AV conditions (Figures 3B and 4D) to define two 'prototypical' activation patterns associated with the two distinct processing stages (Figures 5C and 6C). We then fitted these prototypes to the individual activation patterns from the additional decoding analyses using separate linear models to assess their relative contributions. For each time course independently, as well as for the difference between them, clusters were defined as consecutive time points where the correlation significantly exceeded 0 (paired t-test with $\alpha = 0.05$). The cumulative t-values within each cluster were then compared to the maximum sum derived from surrogate clusters (permutations = 10'000). Time points were considered statistically significant if the probability in the surrogate data was <0.05 for the corresponding clusters. This analysis confirmed that each decoding result was dominated by a single topography (Figures 5C and 6C). This was further complemented by the estimation of Cohen's *d* for the difference between each activation pattern and zero at the level of individual electrodes and time points, which highlighted a single, consistent pattern across each significant time window (Figures 5B and 6B).

Acknowledgments

We sincerely thank Marc Repnow for his excellent technical support. We are also grateful to the Reviewers for their valuable comments and suggestions, which have greatly improved the quality of our manuscript.

References

Ablin, P., Cardoso, J.-F., & Gramfort, A. (2017a). *Faster ICA under orthogonal constraint*. https://doi.org/10.48550/ARXIV.1711.10873

Ablin, P., Cardoso, J.-F., & Gramfort, A. (2017b). *Faster independent component analysis by preconditioning with Hessian approximations*. https://doi.org/10.48550/ARXIV.1706.08171

Akyürek, E. G., & Wolff, M. J. (2016). Extended temporal integration in rapid serial visual presentation: Attentional control at Lag 1 and beyond. *Acta Psychologica*, *168*, 50–64. https://doi.org/10.1016/j.actpsy.2016.04.009

Aru, J., Bachmann, T., Singer, W., & Melloni, L. (2012). Distilling the neural correlates of consciousness. *Neuroscience & Biobehavioral Reviews*, *36*(2), 737–746. https://doi.org/10.1016/j.neubiorev.2011.12.003

Baars, B. J. (2002). The conscious access hypothesis: Origins and recent evidence. *Trends in Cognitive Sciences*, *6*(1), 47–52. https://doi.org/10.1016/S1364-6613(00)01819-2

Bach, M. (1996). The Freiburg Visual Acuity Test—Automatic Measurement of Visual Acuity: *Optometry and Vision Science*, *73*(1), 49–53. https://doi.org/10.1097/00006324-199601000-00008

Biderman, N., & Mudrik, L. (2018). Evidence for Implicit—But Not Unconscious—Processing of Object-Scene Relations. *Psychological Science*, *29*(2), 266–277. https://doi.org/10.1177/0956797617735745

Block, N. (2007). Consciousness, accessibility, and the mesh between psychology and neuroscience. *Behavioral and Brain Sciences*, *30*(5–6), 481–499. https://doi.org/10.1017/S0140525X07002786

Blondel, V. D., Guillaume, J.-L., Lambiotte, R., & Lefebvre, E. (2008). Fast unfolding of communities in large networks. *Journal of Statistical Mechanics: Theory and Experiment*, *2008*(10), P10008. https://doi.org/10.1088/1742-5468/2008/10/P10008

Brainard, D. H. (1997). The Psychophysics Toolbox. *Spatial Vision*, *10*(4), 433–436.

Breitmeyer, B. G., & Öğmen, H. (2007). *Visual masking: Time slices through conscious and unconscious vision* (Second edition). Oxford University Press.

Chiappini, E., Sel, A., Hibbard, P. B., Avenanti, A., & Romei, V. (2022). Increasing interhemispheric connectivity between human visual motion areas uncovers asymmetric sensitivity to horizontal motion. *Current Biology*, *32*(18), 4064-4070.e3. https://doi.org/10.1016/j.cub.2022.07.050

Choi, H., & Scholl, B. J. (2006). Perceiving Causality after the Fact: Postdiction in the Temporal Dynamics of Causal Perception. *Perception*, *35*(3), 385–399. https://doi.org/10.1068/p5462

Cohen, M. A., Dembski, C., Ortego, K., Steinhibler, C., & Pitts, M. (2024). Neural signatures of visual awareness independent of postperceptual processing. *Cerebral Cortex*, *34*(11), bhae415. https://doi.org/10.1093/cercor/bhae415

Cohen, M. A., Ortego, K., Kyroudis, A., & Pitts, M. (2020). Distinguishing the Neural Correlates of Perceptual Awareness and Postperceptual Processing. *The Journal of Neuroscience*, *40*(25), 4925–4935. https://doi.org/10.1523/JNEUROSCI.0120-20.2020

Corballis, P. M. (2003). Visuospatial processing and the right-hemisphere interpreter. *Brain and Cognition*, *53*(2), 171–176. https://doi.org/10.1016/S0278-2626(03)00103-9

Dainton, B. (2023). *Temporal Consciousness*. https://plato.stanford.edu/archives/spr2023/entries/consciousness-temporal/

de Cheveigné, A., & Arzounian, D. (2018). Robust detrending, rereferencing, outlier detection, and inpainting for multichannel data. *NeuroImage*, *172*, 903–912. https://doi.org/10.1016/j.neuroimage.2018.01.035

Dehaene, S., & Changeux, J.-P. (2011). Experimental and Theoretical Approaches to Conscious Processing. *Neuron*, *70*(2), 200–227. https://doi.org/10.1016/j.neuron.2011.03.018

Dehaene, S., Changeux, J.-P., Naccache, L., Sackur, J., & Sergent, C. (2006). Conscious, preconscious, and subliminal processing: A testable taxonomy. *Trends in Cognitive Sciences*, *10*(5), 204–211. https://doi.org/10.1016/j.tics.2006.03.007

Dehaene, S., Naccache, L., Le Clec'H, G., Koechlin, E., Mueller, M., Dehaene-Lambertz, G., Van De Moortele, P.-F., & Le Bihan, D. (1998). Imaging unconscious semantic priming. *Nature*, *395*(6702), 597–600. https://doi.org/10.1038/26967

Del Cul, A., Baillet, S., & Dehaene, S. (2007). Brain Dynamics Underlying the Nonlinear Threshold for Access to Consciousness. *PLoS Biology*, *5*(10), e260. https://doi.org/10.1371/journal.pbio.0050260

Delorme, A., & Makeig, S. (2004). EEGLAB: An open source toolbox for analysis of single-trial EEG dynamics including independent component analysis. *Journal of Neuroscience Methods*, *134*(1), 9–21. https://doi.org/10.1016/j.jneumeth.2003.10.009

Delorme, A., Mullen, T., Kothe, C., Akalin Acar, Z., Bigdely-Shamlo, N., Vankov, A., & Makeig, S. (2011). EEGLAB, SIFT, NFT, BCILAB, and ERICA: New Tools for

Advanced EEG Processing. *Computational Intelligence and Neuroscience*, *2011*, 1–12. https://doi.org/10.1155/2011/130714

Dembski, C., Koch, C., & Pitts, M. (2021). Perceptual awareness negativity: A physiological correlate of sensory consciousness. *Trends in Cognitive Sciences*, *25*(8), 660–670. https://doi.org/10.1016/j.tics.2021.05.009

Dennett, D. C., & Kinsbourne, M. (1992). Time and the observer: The where and when of consciousness in the brain. *Behavioral and Brain Sciences*, *15*(2), 183–201. https://doi.org/10.1017/S0140525X00068229

Drissi-Daoudi, L., Doerig, A., & Herzog, M. H. (2019). Feature integration within discrete time windows. *Nature Communications*, *10*(1), 4901. https://doi.org/10.1038/s41467-019-12919-7

Elliott, M. A., & Giersch, A. (2016). What Happens in a Moment. *Frontiers in Psychology*, *6*. https://doi.org/10.3389/fpsyg.2015.01905

Fahrenfort, J. J., Van Leeuwen, J., Olivers, C. N. L., & Hogendoorn, H. (2017). Perceptual integration without conscious access. *Proceedings of the National Academy of Sciences*, *114*(14), 3744–3749. https://doi.org/10.1073/pnas.1617268114

Fiebelkorn, I. C., Foxe, J. J., Schwartz, T. H., & Molholm, S. (2010). Staying within the lines: The formation of visuospatial boundaries influences multisensory feature integration. *European Journal of Neuroscience*, *31*(10), 1737–1743. https://doi.org/10.1111/j.1460-9568.2010.07196.x

Grootswagers, T., Wardle, S. G., & Carlson, T. A. (2017). Decoding Dynamic Brain Patterns from Evoked Responses: A Tutorial on Multivariate Pattern Analysis Applied to Time Series Neuroimaging Data. *Journal of Cognitive Neuroscience*, *29*(4), 677–697. https://doi.org/10.1162/jocn_a_01068

Harris, J. A., McMahon, A. R., & Woldorff, M. G. (2013). Disruption of Visual Awareness during the Attentional Blink Is Reflected by Selective Disruption of Late-stage Neural Processing. *Journal of Cognitive Neuroscience*, *25*(11), 1863–1874. https://doi.org/10.1162/jocn_a_00443

Haufe, S., Meinecke, F., Görgen, K., Dähne, S., Haynes, J.-D., Blankertz, B., & Bießmann, F. (2014). On the interpretation of weight vectors of linear models in multivariate neuroimaging. *NeuroImage*, *87*, 96–110. https://doi.org/10.1016/j.neuroimage.2013.10.067

Herzog, M. H., Drissi-Daoudi, L., & Doerig, A. (2020). All in Good Time: Long-Lasting Postdictive Effects Reveal Discrete Perception. *Trends in Cognitive Sciences*, *24*(10), 826–837. https://doi.org/10.1016/j.tics.2020.07.001

Herzog, M. H., Kammer, T., & Scharnowski, F. (2016). Time Slices: What Is the Duration of a Percept? *PLOS Biology*, *14*(4), e1002433. https://doi.org/10.1371/journal.pbio.1002433

Holcombe, A. (2014). *The Temporal Organization of Perception* (J. Wagemans, Ed.). Oxford University Press. https://doi.org/10.1093/oxfordhb/9780199686858.013.057

Kayser, S. J., McNair, S. W., & Kayser, C. (2016). Prestimulus influences on auditory perception from sensory representations and decision processes. *Proceedings of the National Academy of Sciences*, *113*(17), 4842–4847. https://doi.org/10.1073/pnas.1524087113

Keuninckx, L., & Cleeremans, A. (2021). The color phi phenomenon: Not so special, after all? *PLOS Computational Biology*, *17*(9), e1009344. https://doi.org/10.1371/journal.pcbi.1009344

Koivisto, M., & Revonsuo, A. (2010). Event-related brain potential correlates of visual awareness. *Neuroscience & Biobehavioral Reviews*, *34*(6), 922–934. https://doi.org/10.1016/j.neubiorev.2009.12.002

Kolers, P. A., & Von Grünau, M. (1976). Shape and color in apparent motion. *Vision Research*, *16*(4), 329–335. https://doi.org/10.1016/0042-6989(76)90192-9

Kouider, S., Stahlhut, C., Gelskov, S. V., Barbosa, L. S., Dutat, M., De Gardelle, V., Christophe, A., Dehaene, S., & Dehaene-Lambertz, G. (2013). A Neural Marker of Perceptual Consciousness in Infants. *Science*, *340*(6130), 376–380. https://doi.org/10.1126/science.1232509

Lau, H. C. (2007). A higher order Bayesian decision theory of consciousness. In *Progress in Brain Research* (Vol. 168, pp. 35–48). Elsevier. https://doi.org/10.1016/S0079-6123(07)68004-2

Ledoit, O., & Wolf, M. (2004). A well-conditioned estimator for large-dimensional covariance matrices. *Journal of Multivariate Analysis*, *88*(2), 365–411. https://doi.org/10.1016/S0047-259X(03)00096-4

Maris, E., & Oostenveld, R. (2007). Nonparametric statistical testing of EEG- and MEG-data. *Journal of Neuroscience Methods*, *164*(1), 177–190. https://doi.org/10.1016/j.jneumeth.2007.03.024

Marti, S., & Dehaene, S. (2017). Discrete and continuous mechanisms of temporal selection in rapid visual streams. *Nature Communications*, *8*(1), 1955. https://doi.org/10.1038/s41467-017-02079-x

McWalter, R., & McDermott, J. H. (2019). Illusory sound texture reveals multi-second statistical completion in auditory scene analysis. *Nature Communications*, *10*(1), 5096. https://doi.org/10.1038/s41467-019-12893-0

Menétrey, M. Q., Herzog, M. H., & Pascucci, D. (2023). Pre-stimulus alpha activity modulates long-lasting unconscious feature integration. *NeuroImage*, *278*, 120298. https://doi.org/10.1016/j.neuroimage.2023.120298

Michel, M., & Doerig, A. (2022). A new empirical challenge for local theories of consciousness. *Mind & Language*, *37*(5), 840–855. https://doi.org/10.1111/mila.12319

Mitroff, S. R., & Scholl, B. J. (2005). Forming and updating object representations without awareness: Evidence from motion-induced blindness. *Vision Research*, *45*(8), 961–967. https://doi.org/10.1016/j.visres.2004.09.044

Mudrik, L., Breska, A., Lamy, D., & Deouell, L. Y. (2011). Integration Without Awareness: Expanding the Limits of Unconscious Processing. *Psychological Science*, *22*(6), 764–770. https://doi.org/10.1177/0956797611408736

Mudrik, L., & Deouell, L. Y. (2022). Neuroscientific Evidence for Processing Without Awareness. *Annual Review of Neuroscience*, *45*(1), 403–423. https://doi.org/10.1146/annurev-neuro-110920-033151

Naccache, L. (2018). Why and how access consciousness can account for phenomenal consciousness. *Philosophical Transactions of the Royal Society B: Biological Sciences*, *373*(1755), 20170357. https://doi.org/10.1098/rstb.2017.0357

Nichols, T. E., & Holmes, A. P. (2002). Nonparametric permutation tests for functional neuroimaging: A primer with examples. *Human Brain Mapping*, *15*(1), 1–25. https://doi.org/10.1002/hbm.1058

Noorman, S., Stein, T., Fahrenfort, J. J., & Van Gaal, S. (2025). Perceptual and attentional impairments of conscious access involve distinct neural mechanisms despite equal task performance. *eLife*, *13*, RP97900. https://doi.org/10.7554/eLife.97900.3

Ojanen, V., Revonsuo, A., & Sams, M. (2003). Visual awareness of low-contrast stimuli is reflected in event-related brain potentials. *Psychophysiology*, *40*(2), 192–197. https://doi.org/10.1111/1469-8986.00021

Otto, T. U. (2006). The flight path of the phoenixVThe visible trace of invisible elements in human vision. *Journal of Vision*, 8.

Otto, T. U., Ögmen, H., & Herzog, M. H. (2009). Feature integration across space, time, and orientation. *Journal of Experimental Psychology: Human Perception and Performance*, *35*(6), 1670–1686. https://doi.org/10.1037/a0015798

Otto, T. U., Ogmen, H., & Herzog, M. H. (2010). Attention and non-retinotopic feature integration. *Journal of Vision*, *10*(12), 8–8. https://doi.org/10.1167/10.12.8

Pilz, K. S., Zimmermann, C., Scholz, J., & Herzog, M. H. (2013). Long-lasting visual integration of form, motion, and color as revealed by visual masking. *Journal of Vision*, *13*(10), 12–12. https://doi.org/10.1167/13.10.12

Pitcher, D. (2022). Visual motion: Asymmetrical processing differences between the cerebral hemispheres. *Current Biology*, *32*(18), R957–R960. https://doi.org/10.1016/j.cub.2022.08.005

Pitts, M. A., Padwal, J., Fennelly, D., Martínez, A., & Hillyard, S. A. (2014). Gamma band activity and the P3 reflect post-perceptual processes, not visual awareness. *NeuroImage*, *101*, 337–350. https://doi.org/10.1016/j.neuroimage.2014.07.024

Railo, H., Koivisto, M., & Revonsuo, A. (2011). Tracking the processes behind conscious perception: A review of event-related potential correlates of visual consciousness. *Consciousness and Cognition*, *20*(3), 972–983. https://doi.org/10.1016/j.concog.2011.03.019

Rimsky-Robert, D., Störmer, V., Sackur, J., & Sergent, C. (2019). Retrospective auditory cues can improve detection of near-threshold visual targets. *Scientific Reports*, *9*(1), 18966. https://doi.org/10.1038/s41598-019-55261-0

Rubinov, M., & Sporns, O. (2010). Complex network measures of brain connectivity: Uses and interpretations. *NeuroImage*, *52*(3), 1059–1069. https://doi.org/10.1016/j.neuroimage.2009.10.003

Scharnowski, F., Ruter, J., Jolij, J., Hermens, F., Kammer, T., & Herzog, M. H. (2009). Long-lasting modulation of feature integrationby transcranial magnetic stimulation. *Journal of Vision*, *9*(6), 1–1. https://doi.org/10.1167/9.6.1

Schlossmacher, I., Dellert, T., Pitts, M., Bruchmann, M., & Straube, T. (2020). Differential Effects of Awareness and Task Relevance on Early and Late ERPs in a No-Report Visual Oddball Paradigm. *The Journal of Neuroscience*, *40*(14), 2906–2913. https://doi.org/10.1523/JNEUROSCI.2077-19.2020

Sergent, C. (2018). The offline stream of conscious representations. *Philosophical Transactions of the Royal Society B: Biological Sciences*, *373*(1755), 20170349. https://doi.org/10.1098/rstb.2017.0349

Sergent, C., Baillet, S., & Dehaene, S. (2005). Timing of the brain events underlying access to consciousness during the attentional blink. *Nature Neuroscience*, *8*(10), 1391–1400. https://doi.org/10.1038/nn1549

Sergent, C., Corazzol, M., Labouret, G., Stockart, F., Wexler, M., King, J.-R., Meyniel, F., & Pressnitzer, D. (2021). Bifurcation in brain dynamics reveals a signature of conscious processing independent of report. *Nature Communications*, *12*(1), 1149. https://doi.org/10.1038/s41467-021-21393-z

Sergent, C., Wyart, V., Babo-Rebelo, M., Cohen, L., Naccache, L., & Tallon-Baudry, C. (2013). Cueing Attention after the Stimulus Is Gone Can Retrospectively Trigger Conscious Perception. *Current Biology*, *23*(2), 150–155. https://doi.org/10.1016/j.cub.2012.11.047

Seth, A. K., & Bayne, T. (2022). Theories of consciousness. *Nature Reviews Neuroscience*, *23*(7), 439–452. https://doi.org/10.1038/s41583-022-00587-4

Sterzer, P., Jalkanen, L., & Rees, G. (2009). Electromagnetic responses to invisible face stimuli during binocular suppression. *NeuroImage*, *46*(3), 803–808. https://doi.org/10.1016/j.neuroimage.2009.02.046

Stiles, N. R. B., Li, M., Levitan, C. A., Kamitani, Y., & Shimojo, S. (2018). What you saw is what you will hear: Two new illusions with audiovisual postdictive effects. *PLOS ONE*, *13*(10), e0204217. https://doi.org/10.1371/journal.pone.0204217

Storm, J. F., Boly, M., Casali, A. G., Massimini, M., Olcese, U., Pennartz, C. M. A., & Wilke, M. (2017). Consciousness Regained: Disentangling Mechanisms, Brain Systems, and Behavioral Responses. *The Journal of Neuroscience*, *37*(45), 10882–10893. https://doi.org/10.1523/JNEUROSCI.1838-17.2017

Subasi, A., & Ismail Gursoy, M. (2010). EEG signal classification using PCA, ICA, LDA and support vector machines. *Expert Systems with Applications*, *37*(12), 8659–8666. https://doi.org/10.1016/j.eswa.2010.06.065

Sun, L., Frank, S. M., Hartstein, K. C., Hassan, W., & Tse, P. U. (2017). Back from the future: Volitional postdiction of perceived apparent motion direction. *Vision Research*, *140*, 133–139. https://doi.org/10.1016/j.visres.2017.09.001

Taylor, M. M., & Creelman, C. D. (1967). PEST: Efficient Estimates on Probability Functions. *The Journal of the Acoustical Society of America*, *41*(4A), 782–787. https://doi.org/10.1121/1.1910407

Thibault, L., van den Berg, R., Cavanagh, P., & Sergent, C. (2016). Retrospective Attention Gates Discrete Conscious Access to Past Sensory Stimuli. *PLOS ONE*, *11*(2), e0148504. https://doi.org/10.1371/journal.pone.0148504

Thorpe, S., Fize, D., & Marlot, C. (1996). Speed of processing in the human visual system. *Nature*, *381*(6582), 520–522. https://doi.org/10.1038/381520a0

Van Gaal, S., De Lange, F. P., & Cohen, M. X. (2012). The role of consciousness in cognitive control and decision making. *Frontiers in Human Neuroscience*, *6*. https://doi.org/10.3389/fnhum.2012.00121

Vogelsang, L., Drissi-Daoudi, L., & Herzog, M. H. (2023). Processing load, and not stimulus evidence, determines the duration of unconscious visual feature integration. *Communications Psychology*, *1*(1), 8. https://doi.org/10.1038/s44271-023-00011-2

Vogelsang, L., Menétrey, M. Q., Drissi-Daoudi, L., & Herzog, M. H. (2024). Investigating the relationship between subjective perception and unconscious feature integration. *Journal of Vision*, *24*(12), 1. https://doi.org/10.1167/jov.24.12.1

Weaver, M. D., Fahrenfort, J. J., Belopolsky, A., & Van Gaal, S. (2019). Independent Neural Activity Patterns for Sensory- and Confidence-Based Information Maintenance during Category-Selective Visual Processing. *Eneuro*, *6*(1), ENEURO.0268-18.2018. https://doi.org/10.1523/ENEURO.0268-18.2018

White, P. A. (2023). Time marking in perception. *Neuroscience & Biobehavioral Reviews*, *146*, 105043. https://doi.org/10.1016/j.neubiorev.2023.105043

Wu, C.-T., Busch, N. A., Fabre-Thorpe, M., & VanRullen, R. (2009). The Temporal Interplay between Conscious and Unconscious Perceptual Streams. *Current Biology*, *19*(23), 2003–2007. https://doi.org/10.1016/j.cub.2009.10.017

Xia, Y., Morimoto, Y., & Noguchi, Y. (2016). Retrospective triggering of conscious perception by an interstimulus interaction. *Journal of Vision*, *16*(7), 3. https://doi.org/10.1167/16.7.3

Ye, M., Lyu, Y., Sclodnick, B., & Sun, H.-J. (2019). The P3 Reflects Awareness and Can Be Modulated by Confidence. *Frontiers in Neuroscience*, *13*, 510. https://doi.org/10.3389/fnins.2019.00510

Data Availability

The data supporting the findings of this study are available on the Open Science Framework (https://osf.io/d83vs/)

Code Availability

All scripts necessary to reproduce the analyses and the figures are available on GitHub (https://github.com/MaelanMenetrey/EEGdecoding_SQM).

Conflict of interest

The authors declare no competing financial interests.

Authors contribution statements

M.Q.M, M.H.H. and D.P. conceived the study; M.Q.M collected the data; M.Q.M and D.P. analyzed the data; M.Q.M, M.H.H. and D.P. interpreted the results; M.Q.M, M.H.H., and D.P. wrote the manuscript.

Supplementary Material

Temporal and cross-condition generalization as a function of the reported vernier (1st or 2nd)

In these supplementary analyses, we decoded the V–AV conditions (V0–AV2 and V0–AV4) from the NV condition, separately for trials in which participants reported the first (i.e., V0) or the second vernier offset (i.e., V2 or V4). The aim was to further corroborate two key points: (1) that the first topography is time-locked to the onset of the first vernier, even in trials where the second vernier dominates the percept and report—indicating unconscious processing; and (2) that the second topography is time-locked to the onset of the perceived (and reported) vernier, as observed in Figure 6A.

The decoder successfully discriminated both V0–AV2 and V0–AV4 trials, regardless of the reported vernier, from NV trials (AUC > 0.5; one-tailed cluster-based permutation test, $p < .05$; Figure S1A). However, the significant decoding windows showed a systematic temporal shift depending on which vernier was reported. When participants reported the first vernier, significant decoding emerged around 200 ms, similar to the analyses including all V–AV trials (vs. NV; Figure 4). In contrast, when the second vernier was reported, the decoding onset was delayed. At first glance, this pattern might appear inconsistent with the interpretation that the initial decoding and first topography are time-locked to the unconsciously processed vernier (which is always V0 in the V–AV conditions).

Because this analysis involved fewer trials due to the split by report, we further assessed the temporal dynamics of the two topographies by correlating the individual activation patterns with the two prototypical topographies identified in the main analyses (Figures 5C and 6C; see Methods). This correlation analysis revealed a significant match with the first topography time-locked to the onset of the first vernier and independent of which vernier was reported, followed by the second topography, which was delayed and extended in duration when participants reported the second vernier (Supplementary Figure S1B). Thus, the first topography—although still evident in the correlation analysis—may not have survived cluster-based permutation correction in the full temporal generalization matrices.

Together, these findings replicate and extend the main results: the first topography is associated with unconscious processing, time-locked to the physical onset of the first vernier (Figures 3C and 4E), whereas the second topography reflects the neural correlate of the consciously perceived vernier offset (Figure 6A).

In a final supplementary analysis, we decoded V-AV conditions, again separately as a function of the reported vernier, from NV conditions but using classifiers trained on V

conditions (V0, V2 or V4 vs. NV). Only V trials where the reported vernier offset was correct were included to ensure that any decoding results could be linked to conscious processing. This approach served two purposes:

(1) to confirm that a single vernier offset is consistently represented in V-AV conditions, even when the reported percept does not match the first offset (V0); and (2) to assess whether the temporal decoding delays previously observed in V conditions (see Figures 2B and 2C) also emerge in V-AV conditions, and whether such delays depend systematically on the spatio-temporal location of the reported vernier.

The cross-condition results successfully decoded V-AV conditions from the NV condition in all cases (AUC above 0.5, one-tailed cluster-based permutation test, $p < .05$; Supplementary Figure S1C). These results confirm that the EEG patterns related to the V-AV and NV conditions differ (see also Figure 4A) and that a single, integrated vernier is consciously perceived when two opposite verniers are presented (see also Figure 4F). Moreover, they demonstrate that temporal shifts in decoding between training and testing sets, as indicated by significant clusters that are not aligned along the diagonal, directly depend on whether the first or second vernier is reported (Supplementary Figure S1C). For example, when classifiers trained on V2 or V4 were tested on the V0-AV4 condition, significant decoding clusters appeared primarily below the diagonal; Supplementary Figure S1C, lower row), indicating faster decoding in the testing set when the first (central) vernier was reported. This effect was more pronounced for classifiers trained on V4 than on V2. Conversely, when the second vernier was reported in the V0-AV4 condition, the significant decoding cluster appeared above the diagonal with classifiers trained on V2, indicating delayed decoding in the testing set. Lastly, classifiers trained on V4 led to a significant decoding cluster aligned along the diagonal, confirming the absence of temporal shift.

Together, these results confirm that the neural processes underlying V–AV conditions—regardless of which vernier is reported—closely resemble those observed in V conditions, following a similar sequence of unconscious and conscious processing stages (see Figures 2 and 3 for comparison). Moreover, they indicate that the temporal dynamics of these processes, particularly those associated with the second topography, vary as a function of the perceptual outcome—that is, depending on which vernier offset dominates the final percept and behavioral report.

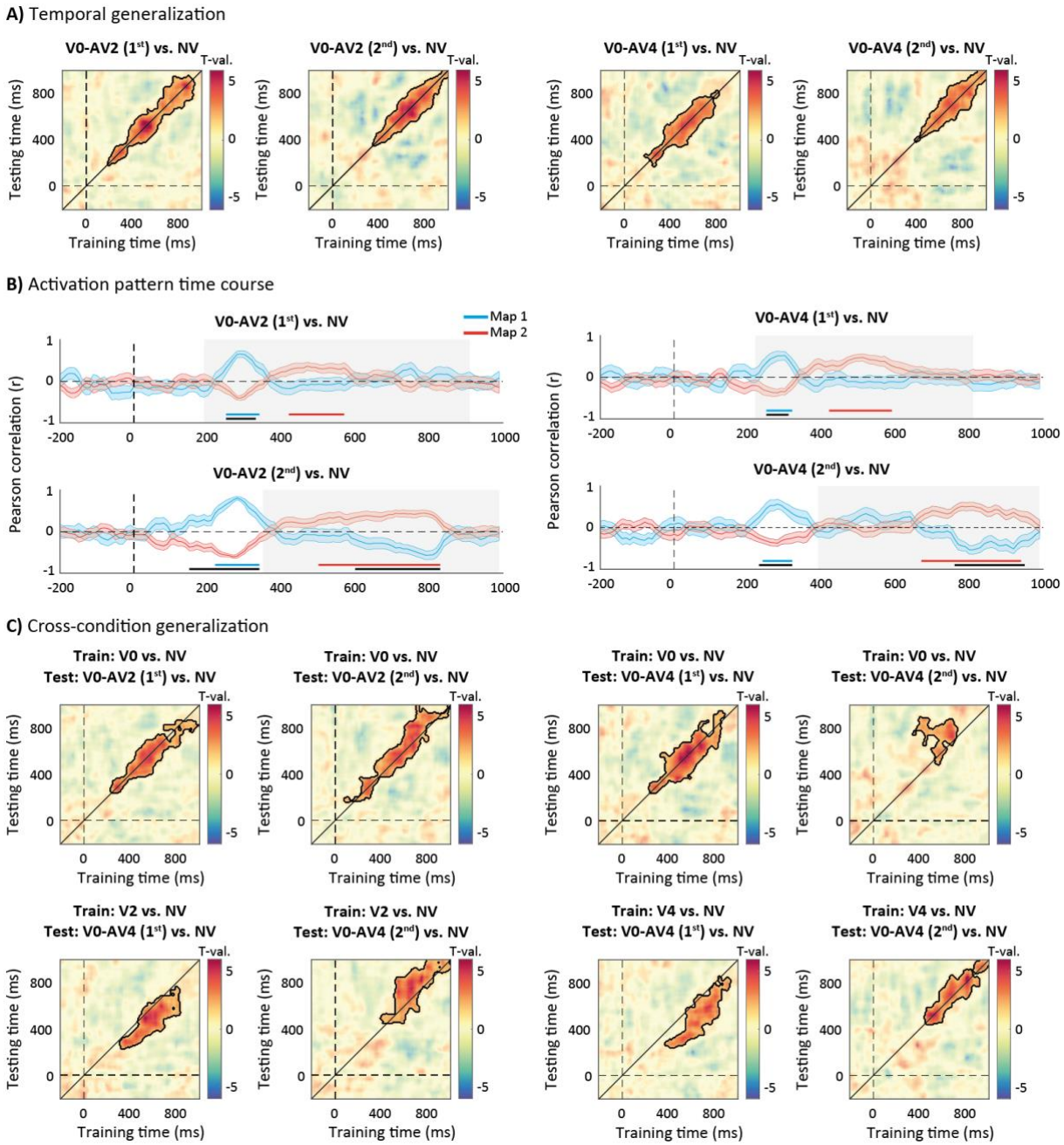

Supplementary Figure S1. Linear discriminant analysis (LDA) with temporal and cross-condition generalization to decode conditions with two opposite verniers and no vernier. Decoding was applied separately on the V-AV trials where the first or the second vernier was reported A) Temporal generalization matrices showing that classifiers successfully discriminate the conditions (V0-AV2 or V0-AV4 vs. NV), regardless of the reported vernier (1st or 2nd). Significant clusters are highlighted (AUC > 0.5, one-tailed cluster-based permutation test, $p < .05$). B) Prototypical activation patterns (Figures 5C and 6C), corresponding to the average of the two distinct activation patterns identified via dissimilarity matrix analysis for all V or V-AV vs. NV contrasts (Figures 3B and 4D, see Methods), were temporally correlated with the activation patterns found in each decoding window (the gray area highlights the significant window found in S1A). Blue and red lines represent the first and second topographies, respectively, and the shaded areas indicate SEM. Significant correlations are also highlighted in blue for the first map or in red for the second (Pearson's $r > 0$, one-tailed cluster-based permutation test, $p < .05$), while significant differences between the two time courses are shown in black (two-tailed cluster-based permutation test, $p < .05$). C) Cross-condition generalization matrices showing that classifiers trained with V conditions (V0, V2 or V4) vs. NV condition successfully discriminate between the two V-AV conditions (V0-AV2 or V0-AV4 vs. NV), regardless of the reported vernier (1st or 2nd). Significant clusters are highlighted (AUC > 0.5, one-tailed cluster-based permutation test, $p < .05$).